

Hyperfine-mediated effects in a Lu⁺ optical clock

Zhang Zhiqiang,^{1,*} K. J. Arnold,^{1,2} R. Kaewuam,¹ M. S. Safronova,^{3,4} and M. D. Barrett^{1,5,†}

¹Centre for Quantum Technologies, 3 Science Drive 2, 117543 Singapore

²Temasek Laboratories, National University of Singapore, 5A Engineering Drive 1, 117411 Singapore

³Department of Physics and Astronomy, University of Delaware, Newark, Delaware 19716, USA

⁴Joint Quantum Institute, National Institute of Standards and Technology and the University of Maryland, College Park, Maryland 20742, USA

⁵Department of Physics, National University of Singapore, 2 Science Drive 3, 117551 Singapore



(Received 13 September 2020; accepted 6 November 2020; published 30 November 2020)

We consider hyperfine-mediated effects for clock transitions in ¹⁷⁶Lu⁺. Mixing of fine-structure levels due to the hyperfine interaction brings about modifications to the Landé *g*-factors and the quadrupole moment for a given state. Explicit expressions are derived for both the *g*-factor and quadrupole corrections, for which leading-order terms arise from the nuclear magnetic dipole coupling. High accuracy measurements of the *g*-factors for the ¹S₀ and ³D₁ hyperfine levels are carried out, and they provide an experimental determination of the leading-order correction terms.

DOI: [10.1103/PhysRevA.102.052834](https://doi.org/10.1103/PhysRevA.102.052834)

I. INTRODUCTION

Singly ionized lutetium (¹⁷⁶Lu⁺) is a unique optical clock candidate in that it provides three possible clock transitions. Of particular interest in this work is the ¹S₀ ↔ ³D₁ transition at 848 nm, which has favorable clock properties relative to leading clock candidates [1]. At the Doppler cooling limit, the ³D₁ ↔ ³P₀ cooling transition provides a fractional second-order Doppler shift below 10⁻¹⁹. The large atomic mass and additional clock transitions allow micromotion shifts to be controlled to a similar level. The blackbody radiation (BBR) shift of the 848-nm transition is $-1.36(10) \times 10^{-18}$ at 300 K, which is the lowest of any optical clock system [1] and easily controllable to the low 10⁻¹⁹ with modest technical effort. More recently, experiments have demonstrated the potential for clock operation with multiple ions, which will ultimately provide improved stability [2,3]. Thus it can be anticipated that this transition will ultimately provide an error budget competitive with leading systems.

A crucial consideration for clock implementation with ¹⁷⁶Lu⁺ is the use of hyperfine averaging in which a reference frequency is defined by an average over all hyperfine states with a common magnetic quantum number, *m* [4]. Provided $|m| < I - J$, where *I* is the nuclear spin and *J* is the electronic angular momentum, the averaging realizes an effective *J* = 0 level and practically eliminates dominant Zeeman shifts and shifts arising from rank 2 tensor interactions, such as the electric quadrupole moment [4]. The averaging principle holds even when there is a large amount of Zeeman mixing within a given fine-structure level, but it omits hyperfine-mediated mixing with other levels. Such mixing influences *g*-factors [5] and is the mechanism for the nonzero quadrupole moment of

³P₀ clock states in Al⁺ and In⁺ [6]. Consequently, it can be anticipated that similar effects will occur for ¹⁷⁶Lu⁺ and likely influence the effectiveness of hyperfine averaging.

In this paper, the influence of hyperfine-mediated mixing on the clock states of ¹⁷⁶Lu⁺ is investigated via high accuracy measurements of *g*-factors for the ¹S₀ and ³D₁ hyperfine levels. Comparison with theoretical results provides an experimental determination of the leading-order correction terms, which arise from the nuclear magnetic dipole coupling. As similar corrections also apply to the quadrupole moments of ³D₁ states, the measurements also allow a reasonable estimate for the residual quadrupole moment arising from hyperfine averaging. Although the corresponding shift of the clock frequency will likely be well below 10⁻¹⁸, it will inevitably be an important consideration for upcoming clock assessments for this atom.

II. EXPERIMENT

A. Apparatus

The relevant level structure of ¹⁷⁶Lu⁺ and the laser systems required are shown in Figs. 1(a) and 1(b). Lasers at 350, 895, and 622 nm provide optical pumping to the ³D₁ state. A laser at 646 nm provides Doppler cooling and state detection for the ³D₁ state with fluorescence collected onto either a single photon counting module (SPCM) or an EMCCD camera. An additional π-polarized 646-nm laser addressing *F* = 7 to *F*' = 7 facilitates state preparation into $|\sup{3}D_1, 7, 0\rangle$. A clock laser at 848 nm drives the ¹S₀-³D₁ clock transition. Two microwave antennas are used to drive the Δ*m* = 0, ±1 microwave transitions indicated in Fig. 1(b). On their respective microwave transitions, each antenna was positioned by hand to give approximately equal coupling to the Δ*m* = ±1 transitions and reduced coupling for Δ*m* = 0.

*e0000155@u.nus.edu

†phybmd@nus.edu.sg

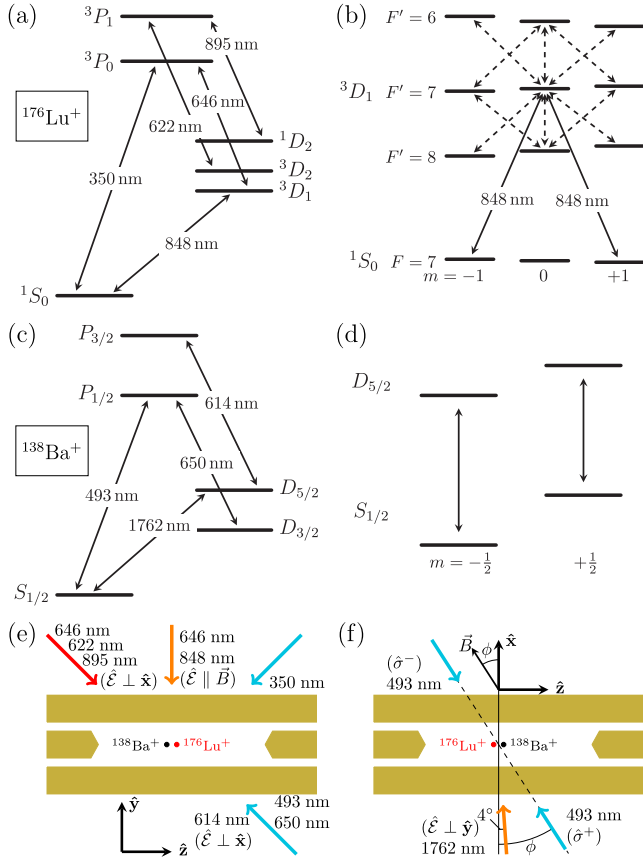


FIG. 1. Schematic of the experimental implementation. Level structures of (a) $^{176}\text{Lu}^+$ and (c) $^{138}\text{Ba}^+$. (b,d) Clock transitions used in this work from which Zeeman splittings are inferred. Dashed lines are microwave transitions. (e),(f) Polarizations and geometric orientations of lasers.

The relevant level structure of $^{138}\text{Ba}^+$ and the laser systems required are shown in Figs. 1(c) and 1(d). Doppler cooling is achieved by driving 493- and 650-nm transitions with fluorescence at 650 nm collected for state detection. The $D_{5/2}$ level is populated by driving the clock transition at 1762 nm and depopulated by optical pumping on the 614-nm transition. State preparation into $m = \pm\frac{1}{2}$ states of $S_{1/2}$ is provided by two additional σ^\pm -polarized 493-nm beams.

The 848-nm clock laser is locked to a 10-cm-long ultralow expansion (ULE) cavity that has a finesse of $\sim 4 \times 10^5$, which provides a laser linewidth of ~ 1 Hz. The 1762-nm laser is phase-locked to an optical frequency comb (OFC), which is itself phase-locked to the 848-nm laser. The short-term stability ($\lesssim 10$ s) of the OFC is thus derived from the ULE cavity. On longer timescales ($\gtrsim 10$ s) the OFC is steered to an active hydrogen maser (HM) reference. All rf and microwave sources are referenced to the HM.

The configurations and polarizations of all laser beams relative to the trap are illustrated in Figs. 1(e) and 1(f). For reference purposes, a coordinate system is given where \hat{x} (\hat{y}) is horizontal (vertical) with respect to the table top, and \hat{z} is along the trap axis. The trap is a four-rod linear Paul trap with axial end caps as described in previous work [7]. In this work, the trap drive frequency is 20.57 MHz, and the

measured trap frequencies for a single $^{138}\text{Ba}^+$ are $\sim 2\pi \times (912, 795, 226)$ kHz, with the lowest trap frequency along the trap axis. As shown in Fig. 1(f), a dc magnetic field is applied in the xz -plane at an angle $\phi = 33(2)^\circ$ with respect to \hat{x} , which defines the quantization axis.

B. Measurements

The g -factors of the $^{176}\text{Lu}^+$ 1S_0 ($F = 7$) and 3D_1 ($F = 6, 7, 8$) levels are denoted g_I and g_F , respectively, and they are measured via a comparison of Zeeman splittings. Comparisons between $^{176}\text{Lu}^+$ and $^{138}\text{Ba}^+$ enable determination of $r_6 \equiv g_{\text{Ba}}/g_6$ and $r_8 \equiv g_{\text{Ba}}/g_8$, where $g_{\text{Ba}} \equiv \frac{1}{2}(g[D_{5/2}] - g[S_{1/2}])$. The g -factors for Lu^+ can then be inferred using the accurately known g -factors in $^{138}\text{Ba}^+$ [7,8]. Ratios among g_F and g_8/g_I are measured using a single ion. Together the two sets of experiments provide a complete determination of g_I and g_F as well as consistency checks between the measurements.

The ratios r_6 and r_8 are measured at an applied magnetic field of ~ 1.573 mT. The experiment sequence consists of the following steps: 200 μs preparation of $^{176}\text{Lu}^+$ in 3D_1 , Doppler cooling of $^{138}\text{Ba}^+$ and $^{176}\text{Lu}^+$ for 1 ms, 1 ms of optical pumping $^{138}\text{Ba}^+$ to either $|S_{1/2}, m = \pm\frac{1}{2}\rangle$ and $^{176}\text{Lu}^+$ to $|^3D_1, 7, 0\rangle$, Rabi spectroscopy with a pulse duration of 1.5 ms being performed simultaneously on the $^{138}\text{Ba}^+$ $|D_{3/2}, m = \pm\frac{1}{2}\rangle$ transition and $^{176}\text{Lu}^+$ $|^3D_1, 7, 0\rangle$ to $|^3D_1, 6, \pm 1\rangle$ (or $|^3D_1, 8, \pm 1\rangle$) transition, 8 ms shelving of the remaining $^{176}\text{Lu}^+$ $|^3D_1, 7, 0\rangle$ population to $|^1S_0, 7, \pm 1\rangle$, sequential state detection of $^{138}\text{Ba}^+$ and $^{176}\text{Lu}^+$ for $\lesssim 1$ ms each, and finally preparation of $^{176}\text{Lu}^+$ in the 3D_1 state and detection for 20 ms. The last step detects the position of $^{176}\text{Lu}^+$ in the two-ion crystal using the different photon collection efficiencies for the two possible crystal configurations. The sequence is repeated four times for Rabi interrogation at approximately the half maximum of either side of the respective pair of Zeeman transitions. Every 20 cycles, an integrating servo is updated to track the respective Zeeman splittings for both $^{138}\text{Ba}^+$ and $^{176}\text{Lu}^+$.

To account for possible spatial dependence on the magnetic field, an additional experiment is performed to calibrate the gradient along the crystal axis. This is done using correlation spectroscopy [9,10] on the $|S_{1/2}, \pm\frac{1}{2}\rangle - |D_{3/2}, \pm\frac{1}{2}\rangle$ transition in a two-ion crystal of $^{138}\text{Ba}^+$, similar to previous work [2]. Specifically, Ramsey spectroscopy is performed on both ions for a duration longer than the optical coherence time of the individuals ions, which is limited by the common mode magnetic field noise. The EMCCD camera is used for single shot detection of both ions. The parity, $p_{12} = \langle \sigma_{z,1} \sigma_{z,2} \rangle$, when averaged over all optical phases of the closing Ramsey pulse, is expected to yield $p_{12} = \frac{p_c}{2} \cos[2\pi(f_1 - f_2)T]$, where p_c characterizes the relative coherence between two oscillators, f_i is the resonant frequency of the i th ion, and T is the Ramsey time. Figure 2(a) shows the typical result as a function of Ramsey time. The difference frequency between the ions measured before and after the measurements of r_6 and r_8 was found to be stable at 20.92(8) Hz, which corresponds to a magnetic field gradient of 0.3917(15) mT/m.

The ratios of g_F are found by interleaved measurement of $|^3D_1, F, \pm 1\rangle$ Zeeman splittings via microwave spectroscopy

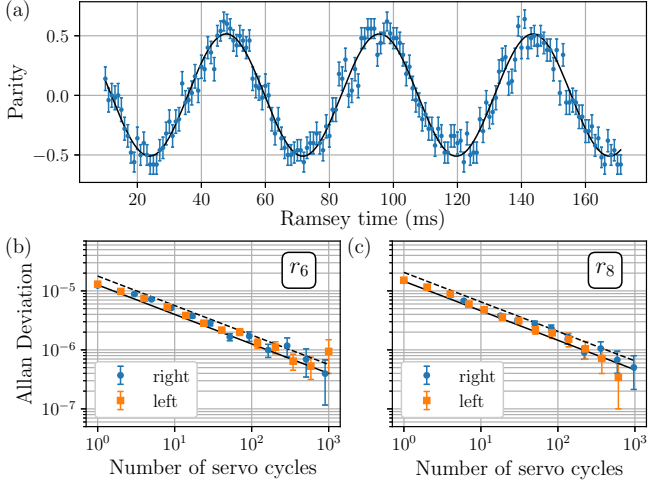


FIG. 2. (a) Correlation spectroscopy of the $|S_{1/2}, \pm\frac{1}{2}\rangle - |D_{3/2}, \pm\frac{1}{2}\rangle$ transition of two $^{138}\text{Ba}^+$ ions. The oscillation frequency of 20.92(8) Hz corresponds to a differential field of 3.73(1) nT between the two ions. (b), (c) Allan deviation of r_6 and r_8 for Lu⁺ on either the left (orange) or right (blue) crystal position. The solid black is the quantum projection noise (QPN) limit. The dashed line is $\sqrt{2}$ above the QPN limit.

on a single Lu⁺ ion with an applied magnetic field of ~ 1.107 mT. The experimental sequence is similar to measurements of r_6 and r_8 but without the Ba⁺ lasers and a longer interrogation time of 16 ms. To probe the Zeeman splitting of the $F = 7$ hyperfine level, additional microwave pulses to transfer from $|^3D_1, 7, 0\rangle$ to $|^3D_1, 6, 0\rangle$ or $|^3D_1, 8, 0\rangle$ are inserted as required. A single cycle consists of sequential Rabi interrogation of four Zeeman pairs: $|^3D_1, 6, \pm 1\rangle$, $|^3D_1, 8, \pm 1\rangle$, and $|^3D_1, 7, \pm 1\rangle$ twice, starting from either $|^3D_1, 6, 0\rangle$ or $|^3D_1, 8, 0\rangle$ to check for consistency. Every 20 cycles, the four independent servos tracking the Zeeman splittings are updated.

An additional experiment measures the ratio g_8/g_1 by interleaved measurement of the $|^3D_1, 8, \pm 1\rangle$ splitting using a 16 ms interrogation time on the microwave transition and the $|^1S_0, 7, \pm 1\rangle$ splitting using a 45 ms interrogation on the 848 nm optical transitions shown in Fig. 1(b). The 45 ms π -time allows for higher resolution of the much smaller ground-state Zeeman splitting and ensures negligible probe-induced shifts.

The r_6 and r_8 results are summarized in Table I with corrections given for the leading systematic effects. As the ions are observed to swap position every 18 min on average, which is much longer than the servo update period, data are sorted into the two possible crystal configurations. Figures 2(b) and 2(c) show the Allan deviations of r_6 and r_8 collected over the course of 5 h.

At the quantum projection noise (QPN) limit, the Allan deviation for the ratio of Zeeman splittings between two levels can be written as σ_0/\sqrt{M} , where M is the number of servo updates and σ_0 fractional resolution from a single update. For Rabi spectroscopy used here, this can be written

$$\sigma_0 = \frac{1.656\hbar}{2\mu_B B \sqrt{N}} \left(\frac{1}{g_1^2 \tau_1^2} + \frac{1}{g_2^2 \tau_2^2} \right)^{1/2}, \quad (1)$$

TABLE I. Values and uncertainties for r_6 and r_8 including correction for systematic effects: (xx) indicates the uncertainty for a given quantity, and $[-E]$ indicates a power of 10 ($\times 10^{-E}$).

Description	Lu ⁺ left	Lu ⁺ right
r_6 raw	5.5965567(17)	5.5965292(20)
magnetic gradient	-1.3258(51)[-5]	1.3258(51)[-5]
microwave ac Stark	7.41(69)[-7]	7.41(69)[-7]
ac magnetic field	-5.31(12)[-7]	-5.31(12)[-7]
r_6 corrected	5.5965437(17)	5.5965427(20)
r_8 raw	-6.4770416(30)	-6.4770088(22)
magnetic gradient	1.5347(59)[-5]	-1.5347(59)[-5]
microwave ac Stark	6.24(43)[-7]	6.24(43)[-7]
ac magnetic field	6.15(14)[-7]	6.15(14)[-7]
r_8 corrected	-6.4770250(30)	-6.4770229(22)

where μ_B is the Bohr magneton, B is the applied magnetic field, N is the number of interrogations per side of a given transition, g_k are the g -factors for the levels involved, and τ_k are the respective interrogation times. The Allan deviations in Figs. 2(b) and 2(c) are observed to be slightly elevated above the QPN. We attribute this to the magnetic field noise, which is comparable to the QPN for the interrogation time used. To account for this, we take the statistical uncertainty in the resulting mean to be $\sqrt{2}$ above the QPN limit, as indicated by the dashed black lines in Figs. 2(b) and 2(c).

The leading systematic effects are: differential Zeeman shifts arising from the magnetic field gradient; ac Stark shifts from off-resonant microwave couplings in Lu⁺; and shifts in the Ba⁺ Zeeman splittings due to magnetic fields at the trap drive rf [11]. Assessment of the magnetic field gradient has already been discussed, leaving only the shifts from the microwave and trap-induced ac fields.

To evaluate the ac Stark shifts from the microwave probe fields, the polarization components at the ion from each antenna were assessed from the relative coupling strength on $\Delta m = (-1, 0, 1)$ transitions at fixed rf power. For the 1.5 ms π -time used during the measurements of r_6 and r_8 , we estimate the ac Stark shift to be $\pm 0.21(2)$ Hz on the $|^3D_1, 7, 0\rangle - |^3D_1, 6, \pm 1\rangle$ transitions and $\mp 0.13(1)$ Hz for the $|^3D_1, 7, 0\rangle - |^3D_1, 8, \pm 1\rangle$ transitions.

Shifts from the trap-induced ac magnetic fields depend only on the component of the ac field perpendicular to the applied dc field [11]. This is measured from an Autler-Townes splitting exactly as described in previous work [7]. The inferred field amplitude of $B_{\perp} = 1.25(1) \mu\text{T}$ implies a $\mp 0.838(19)$ Hz shift on the $|S_{1/2}, \pm\frac{1}{2}\rangle - |D_{3/2}, \pm\frac{1}{2}\rangle$ transitions at the operating magnetic field of 1.573(1) mT.

Other systematic effects considered include shifts on $^{176}\text{Lu}^+$ arising from the 1762-nm laser, the ac-magnetic field effect on Lu⁺, and shifts on $^{138}\text{Ba}^+$ arising from microwave fields. These shifts are all well below the stated uncertainties and are omitted from the table. After accounting for systematic effects, the ratio results r_6 and r_8 are in statistical agreement for both crystal configurations as seen in Table I. For the final values, we take the weighted mean of results

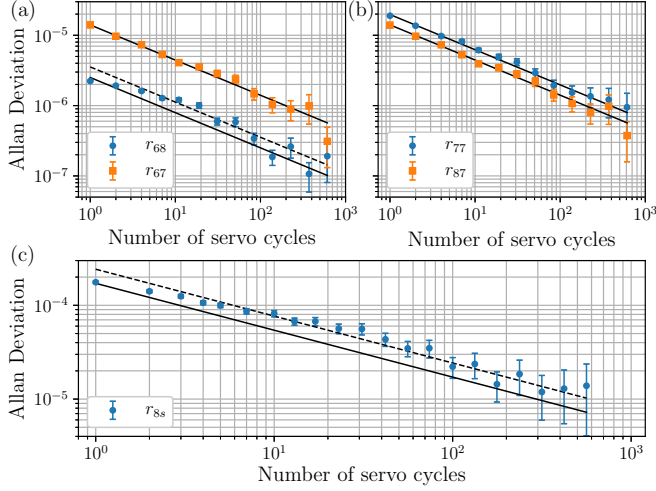


FIG. 3. (a)–(c) Allan deviation of the ratios among g_I , g_F . Solid black lines indicate the QPN limit, and dashed lines are for a factor of $\sqrt{2}$ larger.

for the two crystal configurations. As the measurements are not QPN limited, we use the larger uncertainty from the two configurations in each case, giving

$$r_6 = \frac{g_{\text{Ba}}}{g_6} = 5.596\,543\,3(20), \quad (2a)$$

$$r_8 = \frac{g_{\text{Ba}}}{g_8} = -6.477\,023\,6(30). \quad (2b)$$

Measurements on the single ion yield the following ratios:

$$r_{68} = \frac{g_6}{g_8} = -1.157\,326\,607(88), \quad (3a)$$

$$r_{67} = \frac{g_6}{g_7} = -8.502\,643\,7(24), \quad (3b)$$

$$r_{87} = \frac{g_8}{g_7} = 7.346\,797\,0(20), \quad (3c)$$

$$r_{77} = \frac{g_7}{g_7} = 0.999\,999\,78(38), \quad (3d)$$

$$r_{8s} = \frac{g_8}{g_I} = -254.2897(17), \quad (3e)$$

where r_{77} is the ratio of the $|^3D_1, 7, \pm 1\rangle$ Zeeman splittings measured independently starting from either $|^3D_1, 6, 0\rangle$ or $|^3D_1, 8, 0\rangle$ and is statistically consistent with 1, as expected. The Allan deviations are shown in Figs. 3(a)–3(c). Again, the statistical uncertainties of r_{68} and r_{8s} stated are given as $\sqrt{2}$ larger than the QPN limited uncertainty as indicated by Allan deviations in Figs. 3(a) and 3(c). With microwave and optical interrogation times of 16 and 45 ms, respectively, the systematic effects including shifts caused by the microwave fields and 848-nm light are negligible compared with stated statistical uncertainties.

To check the consistency of the results, r_{68} can be independently evaluated from Eqs. (2a) and (2b) to give $r_{68} = \frac{r_6}{r_8} = -1.157\,325\,74(68)$, which differs from the measured value in Eq. (3a) by $8.7(6.9) \times 10^{-7}$. To determine g_I and g_F , we take the weighted mean of the two values $r_{68} =$

$-1.157\,326\,593(88)$, and

$$g_{\text{Ba}} = \frac{1}{2}[1.200\,367\,31(24) - 2.002\,494\,92(3)] \\ = -0.401\,062\,32(12) \quad (4)$$

determined from reported g -factors for $^{138}\text{Ba}^+$ [7,8]. The values of g_I and g_F are then determined to be

$$g_6 = \frac{g_{\text{Ba}}}{r_6} = -0.071\,662\,506(33), \quad (5a)$$

$$g_7 = \frac{g_{\text{Ba}}}{r_6 r_{68} r_{87}} = 0.008\,428\,261\,9(46), \quad (5b)$$

$$g_8 = \frac{g_{\text{Ba}}}{r_6 r_{68}} = 0.061\,920\,729(29), \quad (5c)$$

$$g_I = \frac{g_{\text{Ba}}}{r_6 r_{68} r_{8s}} = -0.000\,243\,504\,7(16). \quad (5d)$$

III. DISCUSSION

From Appendix A 2, the g -factors for 3D_1 may be written

$$g_6 = -\frac{1}{7}g_J + \frac{8}{7}g_I \\ + \frac{8}{35} \sum_{J'} \beta_{1,J'}^1 - \frac{136}{455} \sum_{J'} \beta_{1,J'}^2 + \delta g_6^{(2)}, \quad (6a)$$

$$g_7 = \frac{1}{56}g_J + \frac{55}{56}g_I \\ + \frac{221}{840} \sum_{J'} \beta_{1,J'}^1 - \frac{17}{280} \sum_{J'} \beta_{1,J'}^2 + \delta g_7^{(2)}, \quad (6b)$$

$$g_8 = \frac{1}{8}g_J + \frac{7}{8}g_I \\ + \frac{7}{40} \sum_{J'} \beta_{1,J'}^1 + \frac{7}{40} \sum_{J'} \beta_{1,J'}^2 + \delta g_8^{(2)}. \quad (6c)$$

Neglecting $\delta g_7^{(2)}$ and using the measured values of g_I and g_F , these equations can be solved for g_J , $\sum_{J'} \beta_{1,J'}^1$, and $\sum_{J'} \beta_{1,J'}^2$, which gives

$$g_J = 0.498\,238\,32(31), \quad (7a)$$

$$\sum_{J'} \beta_{1,J'}^1 = -8.657\,74(41) \times 10^{-4}, \quad (7b)$$

$$\sum_{J'} \beta_{1,J'}^2 = 3.152(13) \times 10^{-5}, \quad (7c)$$

where uncertainties have been propagated from the measurements of g_{Ba} , r_6 , r_{68} , r_{87} , and r_{8s} .

To determine corrections from $\delta g_F^{(2)}$, we first note that they can be expressed in terms of $\beta_{1,2}^k$ and $\langle ^3D_2 \| \mathbf{m} \| ^3D_1 \rangle$, where \mathbf{m} is the magnetic dipole moment operator as defined in Eq. (A5). Both $\sum_{J'} \beta_{1,J'}^1$ and $\sum_{J'} \beta_{1,J'}^2$ are largely determined by the 3D_2 contribution such that they can be used to approximate $\beta_{1,2}^k$ to better than 2%. In addition, calculated matrix elements of \mathbf{m} are typically accurate at the 1% level. Thus, we evaluate $\delta g_F^{(2)}$, as given in Appendix A 2, using $\langle ^3D_1 \| \mathbf{m} \| ^3D_2 \rangle = -2.055\mu_B$ from [12], and Eqs. (7b) and (7c) for $\beta_{1,2}^1$ and $\beta_{1,2}^2$, respectively. The resulting corrected values for the three quantities given in Eqs. (7) are then

$$g_J = 0.498\,236\,6(12), \quad (8a)$$

$$\sum_{J'} \beta_{1,J'}^1 = -8.6574(29) \times 10^{-4}, \quad (8b)$$

$$\sum_{J'} \beta_{1,J'}^2 = 3.130(21) \times 10^{-5}. \quad (8c)$$

As shown in the Appendix, $\delta g_F^{(2)}$ can be written as a sum of two terms: one proportional to a difference in g -factors, and the other proportional to a difference in hyperfine level shifts. As there can be a significant cancellation of the corrections arising from these two contributions, it may well be that additional terms are needed to properly evaluate the corrections. Instead, for all cases, we have used the largest of the resulting two correction terms as the corresponding uncertainty when determining the overall uncertainties given in Eqs. (8). We note that the resulting values in Eqs. (8b) and (8c) are within 3% and 17%, respectively, of the theoretical estimates given in the Appendix, which is reasonable given the estimated uncertainties for calculated matrix elements given in [12].

Finally, the parameter $\beta_{J,J'}^Q$ from Eq. (A28) associated with hyperfine-mediated quadrupole corrections may be written

$$\beta_{J,J'}^Q = \beta_{1,J'}^1 \frac{\mu_B I \langle J' \| \Theta^{(2)} \| J \rangle}{\langle J' \| \mathbf{m} \| J \rangle}. \quad (9)$$

Using the same approximations as above for $\beta_{1,2}^1$ and matrix elements in Appendix A 4, we obtain $\beta_{1,2}^Q = -0.0133ea_0^2$. Thus

$$\langle \delta \Theta(J, F, m) \rangle_F \approx \frac{2}{105} \beta_{1,2}^Q = -2.54 \times 10^{-4} ea_0^2. \quad (10)$$

As measured quadrupole moments are in agreement with theory to within 3%, we would expect the above estimate to be accurate to the 5% level. This represents the effective quadrupole moment for the hyperfine averaged reference frequency for the $^1S_0 - ^3D_1$ clock transition. For a $2\pi \times 200$ kHz dc confinement, this would result in a maximum fractional frequency shift of 7×10^{-19} . In practice, this would be suppressed by the field orientation technique demonstrated in [2], which tunes the spatial dependence to zero leaving predominantly stray field contributions that may not be well aligned to the trap's principal axes.

In summary, we have carried out precision measurements of g -factors for the 1S_0 and 3D_1 levels of $^{176}\text{Lu}^+$. These measurements provide direct evidence of hyperfine-mediated mixing for clock states in $^{176}\text{Lu}^+$, an accurate assessment of $g_J(^3D_1)$, and an estimate of a hyperfine-mediated quadrupole moment that is not canceled by hyperfine-averaging. Although the corresponding shift of the clock frequency will likely be well below 10^{-18} for typical operating conditions, it will inevitably be an important consideration for upcoming clock assessments for this atom.

ACKNOWLEDGMENTS

We thank Sergey Porsev for identifying the correct sign dependencies between the reduced matrix elements. This work is supported by the National Research Foundation, Prime Ministers Office, Singapore and the Ministry of Education, Singapore under the Research Centres of Excellence programme. It is also supported by the National Research

Foundation, Singapore, hosted by National University of Singapore under the Quantum Engineering Programme (Grant Award QEP-P5). M.S.S. acknowledges the sponsorship of ONR Grants No. N00014-17-1-2252 and No. N00014-20-1-2513.

APPENDIX A: THEORY

In this Appendix, relevant theoretical results for g -factor and quadrupole moments are given. Explicit expressions are given for the 3D_1 states, but results can be readily applied to 3D_2 and 1D_2 .

1. Hyperfine interaction theory

From the relativistic treatment in [13], the hyperfine Hamiltonian can be written as a sum of multipole interactions between electrons and nucleons,

$$H_{\text{hfs}} = \sum_{k=1}^{\infty} \mathbf{T}_k^e \cdot \mathbf{T}_k^n, \quad (A1)$$

where \mathbf{T}_k^e and \mathbf{T}_k^n are spherical tensor operators of rank k that operate on the space of electronic and nuclear coordinates, respectively. In the presence of the hyperfine interaction, the total angular momentum $\mathbf{F} = \mathbf{I} + \mathbf{J}$ is conserved, and basis states can be denoted $|\gamma I J F m_F\rangle$, where γ denotes all other quantum numbers. From the Wigner-Eckart theorem, a matrix element of H_{hfs} over the basis set is

$$\begin{aligned} & \langle \gamma' I' J' F' m' | H_{\text{hfs}} | \gamma I J F m \rangle \\ &= \delta_{FF'} \delta_{m'm} (-1)^{J'+I+F} \sum_{k=1}^{k'} \begin{Bmatrix} F & J' & I \\ k & I & J \end{Bmatrix} \\ & \times \langle \gamma' J' \| \mathbf{T}_k^e \| \gamma J \rangle \langle I \| \mathbf{T}_k^n \| I \rangle, \end{aligned} \quad (A2)$$

where $k' = \min(2I, J + J')$. For notational convenience, we will drop γ and I in the notation. As we are primarily concerned with the upper clock states, we will use $J = 1, 2, 3$, and S to denote the triplet and singlet D states.

Following [13], we will use the notation for the ‘‘stretched’’ matrix element of a tensor operator $O_{k,q}$:

$$\begin{aligned} \langle O_k \rangle_I &\equiv \langle II | O_{k,0} | II \rangle \\ &= \begin{pmatrix} I & k & I \\ -I & 0 & I \end{pmatrix} \langle II | O_k \| II \rangle. \end{aligned} \quad (A3)$$

In particular, the nuclear magnetic dipole and electric quadrupole moments are defined as

$$\mu_I = \langle \mathbf{T}_1^n \rangle_I \quad \text{and} \quad Q = 2 \langle \mathbf{T}_2^n \rangle_I. \quad (A4)$$

For a given interaction, H_I , the first-order energy shift $\langle J F m | H_I | J F m \rangle$ is modified by the hyperfine interaction. Following the treatment of the quadrupole moment in [6], the modification can be determined by treating H_I and H_{hfs} on an equal footing in perturbation theory. Explicitly, states are expanded to order n in the hyperfine interaction, and modification to the expectation value of H_I is then attributed to a state-dependent correction to the relevant property of the atom. In considering the importance of various terms, it should be noted that hyperfine interaction terms drop off significantly with k such that $k = 2$ terms at order n can be comparable to $k = 1$ terms at order $n + 1$.

2. Landé g_F -factors

With the Zeeman interaction

$$H_z = -\mathbf{m} \cdot \mathbf{B} = \frac{\mu_B B}{\hbar} (g_L L_z + g_S S_z + g_I I_z), \quad (\text{A5})$$

the term from first-order perturbation theory $\langle JFm|H_z|JFm\rangle$ is the usual weak field Zeeman shift $mg_F\mu_B B$. Corrections derived from n th-order perturbation theory in the hyperfine interaction also have a proportionality to $m\mu_B B$ and thus represent a correction to g_F , which we denote by $\delta g_F^{(n)}$. Up to $n = 1$, we have

$$\begin{aligned} & \langle JFm|H_z|JFm\rangle \\ & + 2 \sum_{J'} \frac{\langle JFm|H_z|J'Fm\rangle \langle J'Fm|H_{\text{hfs}}|JFm\rangle}{E_J - E_{J'}}, \end{aligned} \quad (\text{A6})$$

from which we obtain

$$\delta g_F^{(1)} = 2 \sum_{J'} \frac{\langle JFm|H_z|J'Fm\rangle \langle J'Fm|H_{\text{hfs}}|JFm\rangle}{m\mu_B B(E_J - E_{J'})} \quad (\text{A7})$$

Since H_z is a rank 1 tensor, only couplings to $J' = J \pm 1$ contribute. Using

$$\begin{aligned} & \langle JFm|\mathbf{m}|J'Fm\rangle \\ & = \frac{m(-1)^{F+1+I+J'}(2F+1)}{\sqrt{F(F+1)(2F+1)}} \begin{Bmatrix} F & F & 1 \\ J & J' & I \end{Bmatrix} \langle J\|\mathbf{m}\|J'\rangle, \end{aligned} \quad (\text{A8})$$

and noting that $I + J' + F$ must be integer, we have

$$\begin{aligned} \delta g_F^{(1)} & = 2 \sqrt{\frac{2F+1}{F(F+1)}} \sum_{J',k} \begin{Bmatrix} F & F & 1 \\ J & J' & I \end{Bmatrix} \begin{Bmatrix} F & J' & I \\ I & J & \end{Bmatrix} \\ & \times \frac{\langle J\|\mathbf{m}\|J'\rangle \langle J'\|\mathbf{T}_k^e\|J\rangle \langle I\|\mathbf{T}_k^n\|I\rangle}{\mu_B(E_J - E_{J'})}, \end{aligned} \quad (\text{A9})$$

which may be written

$$\delta g_F^{(1)} = \sum_{k,J'} C_{F,J,J'}^k \beta_{J,J'}^k, \quad (\text{A10})$$

where

$$\beta_{J,J'}^1 = \frac{\langle J\|\mathbf{m}\|J'\rangle \langle J'\|\mathbf{T}_1^e\|J\rangle}{E_J - E_{J'}} \frac{\mu_I}{\mu_B I}, \quad (\text{A11})$$

$$\beta_{J,J'}^2 = \frac{\langle J\|\mathbf{m}\|J'\rangle \langle J'\|\mathbf{T}_2^e\|J\rangle}{E_J - E_{J'}} \frac{Q}{2\mu_B I}, \quad (\text{A12})$$

and

$$\begin{aligned} C_{F,J,J'}^k & = 2I \sqrt{\frac{(2F+1)}{F(F+1)}} \begin{pmatrix} I & k & I \\ -I & 0 & I \end{pmatrix}^{-1} \\ & \times \begin{Bmatrix} F & F & 1 \\ J & J' & I \end{Bmatrix} \begin{Bmatrix} F & J' & I \\ I & J & \end{Bmatrix}. \end{aligned} \quad (\text{A13})$$

For 3D_1 , we have

$$\delta g_6^{(1)} = \frac{8}{35} \sum_{J'} \beta_{1,J'}^1 - \frac{136}{455} \sum_{J'} \beta_{1,J'}^2, \quad (\text{A14a})$$

$$\delta g_7^{(1)} = \frac{221}{840} \sum_{J'} \beta_{1,J'}^1 - \frac{17}{280} \sum_{J'} \beta_{1,J'}^2, \quad (\text{A14b})$$

$$\delta g_8^{(1)} = \frac{7}{40} \sum_{J'} \beta_{1,J'}^1 + \frac{7}{40} \sum_{J'} \beta_{1,J'}^2. \quad (\text{A14c})$$

The dominant contribution is from the M1 coupling to 3D_2 , for which $\beta_{1,2}^1 = -9.1 \times 10^{-4}$, using matrix elements given in Appendix A4. The contribution from 1D_2 is less than 2% of that with $\beta_{1,S}^1 = 1.5 \times 10^{-5}$ and the $k = 2$ corrections from 3D_2 have a similar magnitude with $\beta_{1,2}^2 = 2.6 \times 10^{-5}$. At this few percent level, one should consider next-order corrections, given by

$$\begin{aligned} m\mu_B \delta g_F^{(2)} & = - \sum_{J' \neq J} \sum_{J'' \neq J} \left[\frac{2 \langle JFm|\mathbf{m}|J''Fm\rangle \langle J''Fm|H_{\text{hfs}}|J'Fm\rangle \langle J'Fm|H_{\text{hfs}}|JFm\rangle}{(E_J - E_{J''})(E_J - E_{J'})} \right. \\ & \left. + \frac{\langle JFm|H_{\text{hfs}}|J''Fm\rangle \langle J''Fm|\mathbf{m}|J'Fm\rangle \langle J'Fm|H_{\text{hfs}}|JFm\rangle}{(E_J - E_{J''})(E_J - E_{J'})} \right] \\ & + \langle JFm|\mathbf{m}|JFm\rangle \sum_{J' \neq J} \frac{|\langle JFm|H_{\text{hfs}}|J'Fm\rangle|^2}{(E_J - E_{J'})^2} + 2 \langle JFm|H_{\text{hfs}}|JFm\rangle \sum_{J' \neq J} \frac{\langle JFm|\mathbf{m}|J'Fm\rangle \langle J'Fm|H_{\text{hfs}}|JFm\rangle}{(E_J - E_{J'})^2}. \end{aligned} \quad (\text{A15})$$

For $J = 1$, this is dominated by coupling to 3D_2 for which $J' = J'' = 2$. Hence

$$\delta g_F^{(2)} \approx [g_F(J') - g_F(J)] \frac{|\langle JFm|H_{\text{hfs}}|J'Fm\rangle|^2}{(E_J - E_{J'})^2} + (W_{JF} - W_{J'F}) \frac{2 \langle JFm|\mathbf{m}|J'Fm\rangle \langle J'Fm|H_{\text{hfs}}|JFm\rangle}{(E_J - E_{J'})^2}, \quad (\text{A16})$$

where $W_{JF} = \langle JFm|H_{\text{hfs}}|JFm\rangle$ are the diagonal matrix elements of the hyperfine interaction. Taking only the $k = 1, 2$ contributions for the off-diagonal matrix elements and using the definitions of $\beta_{1,2}^k$, we have

$$\delta g_F^{(2)} \approx [g_F(J') - g_F(J)] \left| \sum_{k=1}^2 \begin{Bmatrix} F & J' & I \\ k & I & J \end{Bmatrix} \begin{pmatrix} I & k & I \\ -I & 0 & I \end{pmatrix}^{-1} \frac{\mu_B I \beta_{J,J'}^k}{\langle J\|\mathbf{m}\|J'\rangle} \right|^2 - \frac{W_{JF} - W_{J'F}}{E_J - E_{J'}} \sum_{k=1}^2 C_{F,J,J'}^k \beta_{J,J'}^k. \quad (\text{A17})$$

Following [14], W_{JF} can be expressed in terms of the measured hyperfine splittings [14,15] and a smaller hyperfine-induced scalar shift common to all F levels of a given J . Neglecting the scalar contributions, we obtain the estimates

$$\delta g_6^{(2)} \approx -3.29 \times 10^{-7}, \quad (\text{A18a})$$

$$\delta g_7^{(2)} \approx 1.10 \times 10^{-8}, \quad (\text{A18b})$$

$$\delta g_8^{(2)} \approx 2.65 \times 10^{-7}, \quad (\text{A18c})$$

where we have approximated g_F using $g_J = 1/2$ and neglected g_I . Hence, $|\delta g_F^{(2)}| \lesssim 1 \times 10^{-3} g_I$.

3. Quadrupole moments

A similar treatment can be applied to determine hyperfine-mediated quadrupole moments. In this case, the resulting quadrupole correction does not average to zero and will thus be a limitation to hyperfine averaging. The analogous expression for the quadrupole correction is

$$\begin{aligned} & \overline{\langle JFm | H_Q | JFm \rangle} \\ &= \langle JFm | H_Q | JFm \rangle \\ &+ 2 \sum_{J'} \frac{\langle JFm | H_Q | J'Fm \rangle \langle J'Fm | H_{\text{hfs}} | JFm \rangle}{E_J - E_{J'}}. \end{aligned} \quad (\text{A19})$$

The first term in this expression is exactly as derived by Itano [16] and can be written

$$\langle JFm | H_Q | JFm \rangle = C_{F,m} \Theta(J) f(\alpha, \beta), \quad (\text{A20})$$

$$\delta \Theta(J, F, m) = 2(2F+1)(-1)^{F-m} \begin{pmatrix} F & 2 & F \\ -m & 0 & m \end{pmatrix} \sum_{J',k} \begin{Bmatrix} F & F & 2 \\ J & J' & I \end{Bmatrix} \begin{Bmatrix} F & J' & I \\ k & I & J \end{Bmatrix} \frac{\langle J || \Theta^{(2)} || J' \rangle \langle J' || \mathbf{T}_k^e || J \rangle \langle I || \mathbf{T}_k^n || I \rangle}{E_J - E_{J'}}. \quad (\text{A26})$$

Taking only the $k = 1$ terms gives

$$\delta \Theta(J, F, m) = 2(2F+1)(-1)^{F-m} \begin{pmatrix} F & 2 & F \\ -m & 0 & m \end{pmatrix} \begin{pmatrix} I & 1 & I \\ -I & 0 & I \end{pmatrix}^{-1} \sum_{J'} \begin{Bmatrix} F & F & 2 \\ J & J' & I \end{Bmatrix} \begin{Bmatrix} F & J' & I \\ 1 & I & J \end{Bmatrix} \beta_{J,J'}^Q, \quad (\text{A27})$$

where

$$\beta_{J,J'}^Q = \frac{\langle J || \Theta^{(2)} || J' \rangle \langle J' || \mathbf{T}_1^e || J \rangle}{E_J - E_{J'}} \mu_I. \quad (\text{A28})$$

For 3D_1 , the only contributions are from 3D_2 and 1D_2 . For the $m = 0$ states of interest,

$$\delta \Theta(J, 6, 0) = -\frac{16}{175} \sum_{J'} \beta_{1,J'}^Q, \quad (\text{A29a})$$

$$\delta \Theta(J, 7, 0) = \frac{1}{35} \sum_{J'} \beta_{1,J'}^Q, \quad (\text{A29b})$$

$$\delta \Theta(J, 8, 0) = \frac{3}{25} \sum_{J'} \beta_{1,J'}^Q. \quad (\text{A29c})$$

where

$$\begin{aligned} C_{F,m} &= (-1)^{2F+I+J-m} (2F+1) \\ &\times \begin{pmatrix} F & 2 & F \\ -m & 0 & m \end{pmatrix} \begin{Bmatrix} F & F & 2 \\ J & J & I \end{Bmatrix} \begin{pmatrix} J & 2 & J \\ -J & 0 & J \end{pmatrix}^{-1}, \end{aligned} \quad (\text{A21})$$

$\Theta(J)$ is the usual quadrupole moment for the fine-structure level defined by

$$\Theta(J) = \begin{pmatrix} J & 2 & J \\ -J & 0 & J \end{pmatrix} \langle J || \Theta^{(2)} || J \rangle, \quad (\text{A22})$$

and $f(\alpha, \beta)$ is determined by the orientation and strength of the applied external field. With the potential in the principal axis frame given by

$$\phi = A[x^2 + y^2 - 2z^2 + \epsilon(x^2 - y^2)], \quad (\text{A23})$$

we have

$$f(\alpha, \beta) = -A[(3 \cos^2 \beta - 1) - \epsilon \sin^2 \beta (\cos^2 \alpha - \sin^2 \alpha)], \quad (\text{A24})$$

where α and β are the Euler angles as defined in [16].

The matrix element $\langle JFm | H_Q | J'Fm \rangle$ can be found in the same way as Eq. (A20) giving

$$\begin{aligned} & \langle JFm | H_Q | J'Fm \rangle \\ &= (-1)^{2F+I+J'-m} (2F+1) \\ &\times \begin{pmatrix} F & 2 & F \\ -m & 0 & m \end{pmatrix} \begin{Bmatrix} F & F & 2 \\ J & J' & I \end{Bmatrix} \langle J || \Theta^{(2)} || J' \rangle f(\alpha, \beta). \end{aligned} \quad (\text{A25})$$

As it has the same orientation dependence as Eq. (A20), the correction can be viewed as a change in the state-dependent quadrupole moment $\Theta(J, F, m) = C_{F,m} \Theta(J)$ by $\delta \Theta(J, F, m)$, which may be written

The average over F is given by

$$\langle \delta \Theta(J, F, m) \rangle = \frac{2}{105} \sum_{J'} \beta_{1,J'}^Q, \quad (\text{A30})$$

which is independent of m at this level of approximation. The dominant term is again the 3D_2 contribution for which $\beta_{1,2}^Q = -0.014$. Omitting the 1D_2 contribution, we get a theoretical estimate of $-2.63 \times 10^{-4} e a_0^2$ for the effective quadrupole moment of the hyperfine-averaged transition.

4. Matrix elements

Matrix elements used in this work are from results reported in Refs. [12,14]. However, signs of matrix elements are not

TABLE II. Reduced matrix elements used in this work. These are derived from the work in Ref. [12] and include the relative sign. Matrix elements of T_1^e and T_2^e are specified in MHz/ μ_N and MHz/b, where μ_N is the nuclear magnetic moment and b is the barn unit of area. Matrix elements of \mathbf{m} and $\Theta^{(2)}$ are given in units of μ_B and ea_0^2 , respectively, where μ_B is the Bohr magneton, e is the fundamental unit of charge, and a_0 is the Bohr radius.

ME	Value	ME	Value
$\langle {}^3D_2 \ T_1^e \ {}^3D_1 \rangle$	-18 682	$\langle {}^1D_2 \ T_1^e \ {}^3D_1 \rangle$	10 618
$\langle {}^3D_2 \ T_2^e \ {}^3D_1 \rangle$	686	$\langle {}^1D_2 \ T_2^e \ {}^3D_1 \rangle$	70
$\langle {}^3D_1 \ \mathbf{m} \ {}^3D_2 \rangle$	-2.055	$\langle {}^3D_1 \ \mathbf{m} \ {}^1D_2 \rangle$	-0.524
$\langle {}^3D_1 \ \Theta^{(2)} \ {}^3D_2 \rangle$	-4.523	$\langle {}^3D_1 \ \Theta^{(2)} \ {}^1D_2 \rangle$	-1.018

always specified, as the sign of a single matrix element can be set arbitrarily. As this work explicitly requires the relative sign between matrix elements, we give a list of the relevant matrix elements including the sign in Table II. Matrix elements of T_2^e given in the table differ in sign from those given in [14]. This

was due to a difference in the definition of T_2^e relative to [13] that was discovered in the course of this work. This will result in minor changes to the calculated results in [12,14], but it will not significantly influence the results or conclusions in those reports.

- [1] K. J. Arnold, R. Kaewuam, A. Roy, T. R. Tan, and M. D. Barrett, Blackbody radiation shift assessment for a lutetium ion clock, *Nat. Commun.* **9**, 1650 (2018).
- [2] T. R. Tan, R. Kaewuam, K. J. Arnold, S. R. Chanu, Z. Zhang, M. S. Safronova, and M. D. Barrett, Suppressing Inhomogeneous Broadening in a Lutetium Multi-Ion Optical Clock, *Phys. Rev. Lett.* **123**, 063201 (2019).
- [3] R. Kaewuam, T. R. Tan, K. J. Arnold, S. R. Chanu, Z. Zhang, and M. D. Barrett, Hyperfine Averaging by Dynamic Decoupling in a Multi-Ion Lutetium Clock, *Phys. Rev. Lett.* **124**, 083202 (2020).
- [4] M. D. Barrett, Developing a field independent frequency reference, *New J. Phys.* **17**, 053024 (2015).
- [5] S. G. Porsev, U. I. Safronova, and M. S. Safronova, Theoretical study of the g factor and lifetime of the $6s6p\ ^3P_0$ state of mercury, *Phys. Rev. A* **96**, 012509 (2017).
- [6] K. Beloy, David R. Leibrandt, and Wayne M. Itano, Hyperfine-mediated electric quadrupole shifts in Al^+ and In^+ ion clocks, *Phys. Rev. A* **95**, 043405 (2017).
- [7] K. J. Arnold, R. Kaewuam, S. R. Chanu, T. R. Tan, Z. Zhang, and M. D. Barrett, Precision Measurements of the $^{138}\text{Ba}^+ 6s\ ^2S_{1/2} - 5d\ ^2D_{5/2}$ Clock Transition, *Phys. Rev. Lett.* **124**, 193001 (2020).
- [8] G. Marx, G. Tommaseo, and G. Werth, Precise g_j - and g_i -factor measurements of Ba^+ isotopes, *Eur. Phys. J. D* **4**, 279 (1998).
- [9] M. Chwalla, K. Kim, T. Monz, P. Schindler, M. Riebe, C. F. Roos, and R. Blatt, Precision spectroscopy with two correlated atoms, *Appl. Phys. B* **89**, 483 (2007).
- [10] C.-W. Chou, D. B. Hume, M. J. Thorpe, D. J. Wineland, and T. Rosenband, Quantum Coherence Between two Atoms Beyond $Q = 10^{15}$, *Phys. Rev. Lett.* **106**, 160801 (2011).
- [11] H. C. J. Gan, G. Maslennikov, K.-W. Tseng, T. R. Tan, R. Kaewuam, K. J. Arnold, D. Matsukevich, and M. D. Barrett, Oscillating-magnetic-field effects in high-precision metrology, *Phys. Rev. A* **98**, 032514 (2018).
- [12] E. Paez, K. J. Arnold, E. Hajiyev, S. G. Porsev, V. A. Dzuba, U. I. Safronova, M. S. Safronova, and M. D. Barrett, Atomic properties of Lu^+ , *Phys. Rev. A* **93**, 042112 (2016).
- [13] K. Beloy, A. Derevianko, and W. R. Johnson, Hyperfine structure of the metastable 3P_2 state of alkaline-earth-metal atoms as an accurate probe of nuclear magnetic octupole moments, *Phys. Rev. A* **77**, 012512 (2008).
- [14] R. Kaewuam, T. R. Tan, K. J. Arnold, and M. D. Barrett, Spectroscopy of the $^1S_0 - ^1D_2$ clock transition in $^{176}\text{Lu}^+$, *Phys. Rev. A* **99**, 022514 (2019).
- [15] R. Kaewuam, A. Roy, T. R. Tan, K. J. Arnold, and M. D. Barrett, Laser spectroscopy of $^{176}\text{Lu}^+$, *J. Mod. Opt.* **65**, 592 (2018).
- [16] W. M. Itano, External-field shifts of the $^{199}\text{Hg}^+$ optical frequency standard, *J. Res. Natl. Inst. Stand. Technol.* **105**, 829 (2000).